Hindawi Publishing Corporation
International Journal of Photoenergy
Volume 2006, Article ID 85469, Pages 1–6
DOI 10.1155/IJP/2006/85469

Photoelectrochemical Characterization and Photocatalytic Properties of Mesoporous TiO_2/ZrO_2 Films

Natalie Smirnova,[1] Yuriy Gnatyuk,[1] Anna Eremenko,[1] Gennadiy Kolbasov,[2] Vera Vorobetz,[2] Irina Kolbasova,[3] and Olga Linyucheva[3]

[1] *Institute of Surface Chemistry, Ukrainian National Academy of Sciences, 17 Gen. Naumov str., Kyiv 03164, Ukraine*
[2] *Institute of General & Inorganic Chemistry, Ukrainian National Academy of Sciences, 32/34 Palladin str., Kyiv 03680, Ukraine*
[3] *National Technical University, 37 prosp. Peremogy, Kyiv 03056, Ukraine*

Received 25 February 2005; Revised 10 July 2005; Accepted 28 August 2005

Optically transparent, crack-free mesoporous titania and zirconia-doped titania thin film photocatalysts were fabricated by sol-gel technique, using nonionic amphiphilic block copolymer Pluronic P123 as template. The structural and optical properties of these films were characterized using SEM, low-angle XRD, and UV/Vis spectroscopy, hexane adsorption investigation. Band gap energy and the position of flatband potentials were estimated by photoelectrochemical measurements. Enhancing of photocatalytic activity of zirconia-doped films relative to pure TiO_2 originates from an anodic shift of the valence band edge potential. Catalytic activity of mesoporous TiO_2 and TiO_2/ZrO_2 (5–50% of ZrO_2) films in the processes of Cr^{VI} to Cr^{III} photoreduction and 2,4-dinitroaniline photooxidation correlates with crystalline size and growth with increasing of specific surface area of the samples.

1. INTRODUCTION

Many organic substrates have been shown to be oxidatively (in some cases reductively) degraded and ultimately mineralized completely under UV irradiation on nanosized titania catalysts [1–3]. Catalytic activity, i.e. strongly reductive/oxidative effect of titanium dioxide is based on the electron/hole pair formed upon photoexcitation. A great deal of research has been conducted recently to optimise the performance of the TiO_2 photocatalysts, especially mesoporous films, with high surface area [4–7].

Mixed oxide composite materials can often be more efficient photocatalysts than pure substances. This phenomenon arises through the generation of new active sites due to interactions between titania and dopant oxides, through improved mechanical strength, thermal stability, and surface area of doped titania [8–10] and perhaps to the absence of a rutile phase in the supported oxide samples. Mesoporous TiO_2 and TiO_2/ZrO_2 coatings showed high activity in the gas-phase photooxidation of ethanol and acetone [8, 11].

Fu et al. [12] reported the enhancing of photocatalytic activity of mixed metal oxides (TiO_2/SiO_2 and TiO_2/ZrO_2) compared to TiO_2 for oxidation of ethylene due to increased thermal stability and surface acidity. Also, it was found that the photocatalytic activity depends on the crystalline size and crystalline phases that modify the TiO_2 band gap [3, 13]. Although the knowledge on the band edge position is particularly useful in photocatalysis, the effect of zirconium content in TiO_2/ZrO_2 mixed oxides for their photophysical properties has not been much studied.

Herein, we report on mesoporous TiO_2 and TiO_2/ZrO_2 thin films with 5–30% ZrO_2 content that were prepared via the templating sol-gel route and characterized using SEM, XRD measurements, UV/Vis spectroscopy, and hexane adsorption investigation.

The electronic properties of TiO_2/ZrO_2 photocatalysts such as band gap energy, flat-band potential, and resistivity were measured and correlated with the photocatalytic activities in Cr^{VI} to Cr^{III} photoreduction and 2,4-dinitroaniline oxidation.

2. EXPERIMENTAL

2.1. Preparation of the samples

For the synthesis of TiO_2 and TiO_2/ZrO_2 mesoporous films, titanium and zirconium tetra-iso-propoxides (Aldrich) were used as metal sources. Triblock copolymer $(PEO)_{20}(PPO)_{70}$-$(PEO)_{20}$ (Pluronic P123, BASF) has been used as templating

agent. To control hydrolysis-condensation reaction rates and to prevent oxides precipitation, acetylacetone (acac) was used as a complexing agent. The typical molar ratios TIPT : $Zr(0Pr)_4$: P123 : acac : HCl : H_2O : C_2H_5OH of the reacting solution was 1–0.7 : 0–0.3 : 0.05 : 0.5 : 4.6 : 10 : 41. Dip-coated films on glass substrates were aged for 12 hours at room temperature and calcined by heating at the rate of 1.5 °C/min to 500 °C, and kept for 2 h to remove the block copolymer species and to increase cross-linking of the inorganic framework. For comparison, TiO_2 coatings without template were prepared in parallel.

2.2. Structural and optical characterizations

X-ray diffraction measurements on sintered coatings were performed with a Cu-K_{ff} DRON-4-07 M system (LOMO St. Petersburg) with the minimum glancing angle $\theta = 0.4$. For the SEM measurements, films were prepared on conducting glass substrate coated with SnO_2. The samples were imaged by the LEO 1530 electron microscope.

The Brunauer-Emmett-Teller (BET) surface area and pore size distribution of the thin film coated on covering slides for microscopy were determined from hexane adsorption-desorption isotherms [11], obtained at 20 °C in thermostatting vacuum setup in the relative pressure (P/P_0) range of 0.01–1.00. All samples were degassed at 200 °C prior to measurements.

2.3. The photoelectrochemical properties

The photoelectrochemical properties of the TiO_2/ZrO_2 electrodes were estimated using the spectral dependence of the photoelectrochemical current (i_{ph}), measured with a commercial spectrometer KSVU-1 (LOMO, Russia) with spectral resolution 1 nm. The experiments were carried out at 22 °C under pure argon bubbling in the temperature-controlled quartz cell with optically transparent planar-parallel windows. The i_{ph} spectra were measured with usage of the mechanical light chopper of 20 Hz frequencies and standard circuit synchronous detection followed by computer-assisted spectral analysis. A high-pressure xenon lamp with stabilized discharge current was used as light source. The i_{ph} spectra were expressed in units of quantum efficiency (electron/photon). The resistivity of TiO_2/ZrO_2 films on Ti substrate was measured by means of common alternating current bridge BM401. In parallel, the resistivity of the TiO_2/ZrO_2 films on a glass substrate was measured with the help of a digital multimeter P386, that gives the good reproducibility. Ag/AgCl electrode was used as the reference electrode on the pH value of the electrolyte.

2.4. Photocatalytic activity

Photocatalytic activity of TiO_2 and TiO_2/ZrO_2 films has been checked in the processes of Cr(VI) to Cr(III) photoreduction in water solution of $K_2Cr_2O_7$ ($C_M = 2 \cdot 10^{-4}$ M) in the presence of EDTA ($C_M = 2 \cdot 10^{-4}$ M) at pH = 2 and 2,4-dinitroaniline photooxidation ($C_M = 5 \cdot 10^{-5}$ M). The open reactor with the reaction components (enabled continuous inflow of oxygen) was irradiated with an UV light of mercury lamp PRK-1000 with intensity P_0=3·10^{-7} einstein · dm^{-3} · s^{-1}. Running water was circulated through the jacket to ensure constant temperature of the magnetically stirred reaction mixture. During the experiments, concentration of reagents has been controlled with an UV-VIS spectrometer Perkin-Elmer Lambda-35.

3. RESULTS AND DISCUSSION

3.1. Structural characterization

Prepared by the sol-gel process from the Zr and Ti alkoxides using a template agent, TiO_2/ZrO_2 films on the glass substrates are optically transparent. The thickness of one-coated films calculated ranges between 70–90 nm, refractive indexes 1.9–2.1 [11]. The low-angle X-ray diffraction pattern of as-synthesised films displays 3 peaks in the low-angle range typical for ordered lamellar mesophase. The 500 °C calcined films showed only one peak in the low-range pattern due to a partial collapse of the ordered pore structure. No peaks were seen in the wide-angle XRD pattern. This observation witnesses rather about pore walls contained tiny crystallites not resolvable by conventional wide-angle XRD than about noncrystalline pore walls. XRD patterns of TiO_2/ZrO_2 powders, prepared from film precursors after gelation, were analysed to estimate the structure and crystallite size of samples. When pure TiO_2 and TiO_2/ZrO_2 (5–10%) showed anatase structure with 80% of crystalline phase and mean crystallite size 9–10 nm, increasing of Zr content leads to drop of crystallinity. Only weak reflex at $2\theta = 25.5$ corresponding to anatase is observed for TiO_2/ZrO_2 (30%), while TiO_2/ZrO_2 (50%) is amorphous. As we reported previously [14], no phases associated with pure zirconia were observed, only tetragonal titania anatase was detected in the range of ZrO_2 concentrations of 5–30% after 600 °C calcination. This means that some titanium atoms are substitutes by zirconium in the anatase structure.

The adsorption-desorption isotherms of hexane on 500 °C calcined TiO_2 and TiO_2/ZrO_2 samples demonstrated the type IV shape, which indicates the presence of mesoporosity in accordance with [15]. The specific surface areas (S_{BET}) and mean pore sizes of TiO_2/ZrO_2 films annealed at 500 °C are listed in Table 1. Uniform porosity with $r = 8$–10 nm is typical for samples with low ZrO_2 content. Pure TiO_2 and 30% TiO_2/ZrO_2 films show broader pore size distribution shifted to the larger pores with radius around 14 nm.

The SEM image (Figure 1) of 5% TiO_2/ZrO_2 film presents a well-defined porous structure with pore walls 3–5 nm and effective pore radius $r_{eff} = 6$–8 nm.

From the above results, it is clear that the films with low ZrO_2 (5–10%) concentration are homogeneous with stable mesoporous structure. Decreasing of homogeneity with further increasing of zirconia content up to 30% of ZrO_2 leads to the collapse of porous structure after calcinations.

Table 1: Surface characteristics, rate constants, and half-conversion time for Cr(VI) to Cr(III) photoreduction over TiO_2 and TiO_2/ZrO_2 mesoporous films calcined at 500 °C.

Sample	Sample characteristics		Cr(VI) to Cr(III) photoreduction	
	S_{BET} (m^2/g)	r (nm)	k (min^{-1})	$\tau_{1/2}$** (min)
TiO_2 nonporous*	—	—	$1.31 \cdot 10^{-2}$	53
TiO_2	816	3.8; 6.1; 13.8	$1.88 \cdot 10^{-2}$	37
TiO_2/ZrO_2 (5% ZrO_2)	1007	8.2	$2.33 \cdot 10^{-2}$	30
TiO_2/ZrO_2 (10% ZrO_2)	557	3.8, 9.7	$2.03 \cdot 10^{-2}$	34
TiO_2/ZrO_2 (30% ZrO_2)	123	3.8; 14.2	$1.49 \cdot 10^{-2}$	46

*For film prepared without template, S_{BET} cannot be measured directly.

**Half time of conversion Cr(VI) to Cr(III) in 20 ml of $2 \cdot 10^{-4}$ M water solution of $K_2Cr_2O_7$ in the presence of EDTA ($2 \cdot 10^{-4}$ M) at pH = 2 over 1 film ($m = 0.001$ g).

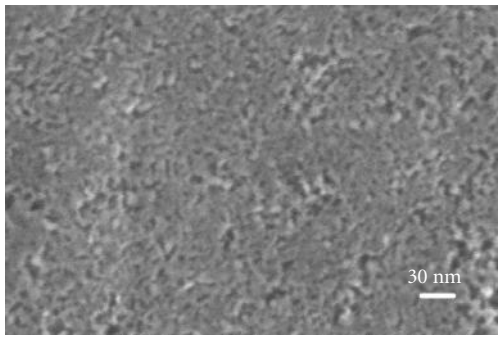

Figure 1: SEM image of 5% TiO_2/ZrO_2 film.

3.2. Photoelectrochemical properties

To obtain the value of the band gap energy, spectral dependences of photocurrent were measured for the TiO_2/ZrO_2 electrodes (TiO_2/ZrO_2 films were coated on Ti substrate). It is well known that quantum yield of photoelectrochemical current η in semiconductors can be expressed as [16] $\eta = (A/h\nu)(h\nu - E_g)^m$, where $h\nu$ is the photon energy, $m = 1/2$ for the direct transition, and $m = 2$ for the indirect transition.

For the tested TiO_2/ZrO_2 compositions, we cannot obtain linear dependence in $(\eta \cdot h\nu)^{1/2} = f(h\nu)$ coordinates, that were possibly connected with some reasons such as: photocurrent in the longwave spectral region caused by defects in the anatase structure, low intensity of photocurrent corresponded to indirect transition in thin films due to low absorption coefficient. Photocurrent spectra were presented as $(\eta \cdot h\nu)^2 = f(h\nu)$ dependence, which was linear in the wide range of wavelength. As follows from the result presented in Figure 2a, experimental data fit better to a direct transition. Band gap (E_g) values were calculated by extrapolation of straight line of these dependences to the abscissa (Table 2). With growing of zirconium content, band gap increases from 3.17 for TiO_2 to 3.45 eV for TiO_2/ZrO_2 (50%) was obtained that can been attributable to quantum-size effect [17]. Our data agreed with diverse literature (E_g = 3.4–3.9 eV for the different nanocrystals size and measurement technique). This result indicates that zirconum doping in TiO_2 inhibits crystallite growing [9, 10]. Crystallite sizes calculated in accordance with [18] are listed in Table 2. To test whether the larger band gap is caused by a shift of the valence (E_v) or conduction (E_c) band edges, the position of the flatband potential (U_{fb}) of the catalysts was determined by the direct electrochemical measurements of photocurrent as a function of applied potential in aqueous 0.5 NaCl.

Flatband potentials were estimated from i_{ph} changes measured at the photocurrency maximum for TiO_2 and TiO_2/ZrO_2 films coated on the titanium substrate in aqueous 0.5 M NaCl plotted against applied potential by extrapolation of straight line of these dependences to the abscissa (Figure 2b). Flatband potential values for the samples with different zirconium content differ insignificantly and are comparable with the value of −(0.47–0.49) V, obtained at pH ≈ 7 for nitrogen-doped titanium dioxide [19] and $U_{fb} = -0.58$ V measured for anatase single crystal [20].

Resistivity of films was measured for evaluation of relative shift of the bottom of the conduction band (ΔE_c) and the upper edge of the valence band (ΔE_c) positions relative to pure TiO_2 depending on Zr content. The difference (ΔE_{fc}) between electrochemical potential of the electrodes (Fermi level potential), that corresponds to flatband potential, and potential of the bottom of the conduction band $-\Delta E_c$ was calculated using the following equation [21]:

(i) $\Delta E_{fc} = kT/e \ln(N_c/n_0)$, where n_0 and N_c denote concentration of electrons and density of electronic states in the conduction band, respectively.

ΔE_c and ΔE_v values, calculated in assumption, that mobility of electron and N_c do not depend on TiO_2/ZrO_2 ratio, are presented in Table 2:

$$\Delta E_c = E_c - E_c^{TiO_2}, \qquad \Delta E_v = E_v - E_v^{TiO_2}, \qquad E_v = E_c + (e)^{-1} E_g. \tag{1}$$

As followed from Table 2, increase of Zr content leads to anodic shift of the upper edge of the valence band ΔE_v positions, when relative shift of the bottom of the conduction band ΔE_c was not significant. As the location of the valence band is a measure of the oxidation power of the photogenerated holes, we can predict the enhancing of catalytic activity in photooxidation processes.

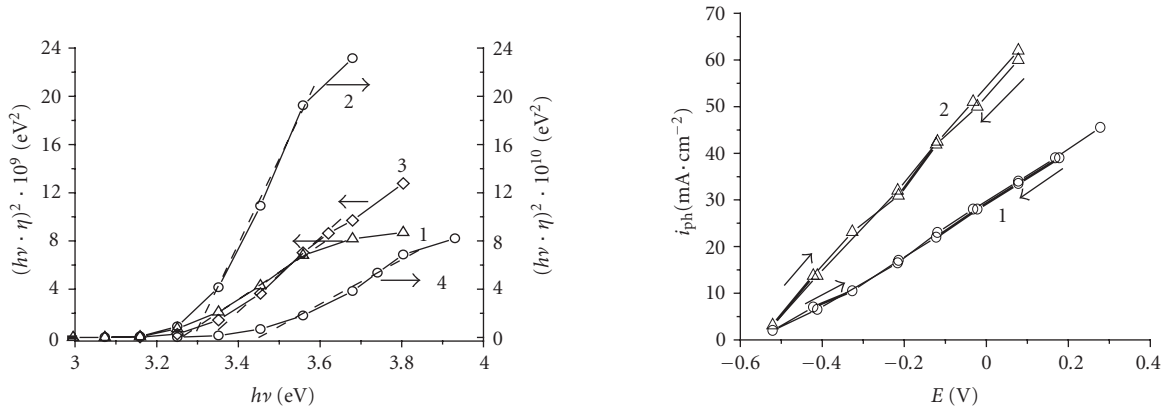

FIGURE 2: (a) $(\eta \cdot h\nu)^2 = f(h\nu)$ dependence for TiO_2/ZrO_2 film: 1–5; 2–10; 3–30; 4–50% of ZrO_2. $E = 0.28$ V (NHE). (b) Photocurrency (i_{ph}) changes plotted against applied potential (versus NHE) for TiO_2/ZrO_2 films: 1–10% Zr; 2–50% Zr content.

TABLE 2: Photoelectrochemical characteristics for TiO_2/ZrO_2 photocatalysts.

Catalyst	E_g (eV)	d (nm)	E_{fb}, [V, NHE]	ρ (Ohm·cm)	ΔE_c (V)	ΔE_v (V)
TiO_2	3.17	9–10	−0.51	$5.7 \cdot 10^7$	0	0
TiO_2/ZrO_2 (5% Zr)	3.26	3.9	−0.52	$8.1 \cdot 10^7$	0.01	0.10
TiO_2/ZrO_2 (10% Zr)	3.29	3.2	−0.54	$4.0 \cdot 10^7$	0.01	0.13
TiO_2/ZrO_2 (30% Zr)	3.33	2.7	−0.55	$2.2 \cdot 10^6$	−0.02	0.14
TiO_2/ZrO_2 (50% Zr)	3.45	1.9	−0.52	$6.5 \cdot 10^7$	0.01	0.29

At the constant electrochemical potential of TiO_2 photocatalytical reactivity of titania coatings can be controlled by electrons concentration in the conductive band, for example, by metal doping.

For high resistive TiO_2 films, we can take into consideration alteration of Fermi quasilevel under illumination, and E_{fb} readjustment as the results of trapping of photogenerated charge carriers on surface electronic states and electronic states in the space charge region of semiconductor [21]. Alteration of Fermi quasilevel in semiconductor depends on light intensity and can be significant (up to 1 V, as was experimentally obtained for $A^{II}B^{VI}$ compounds [22]).

3.3. *Photocatalytic activity of* TiO_2/ZrO_2 *coatings in toxic* Cr(VI) *to nontoxic* Cr(III) *ions photoreduction*

Photocatalytic activity of mesoporous TiO_2/ZrO_2 films has been tested in the photoreduction of toxic Cr(VI) to nontoxic Cr(III) ions in acid water solutions in the presence of environmentally important substrate EDTA (Table 1). This process has been taken as a model of real wastewaters, where oxidants and reductants are present together, for comparable studies of commercial samples and platinized TiO_2 powders [2, 23, 24]. The mechanism of photocatalytic Cr(VI) reduction in the presence of electron scavenger (EDTA, salicylic acid or other organic molecules) is well described in [2, 23, 24].

In Figure 3, we show the changes in Cr(VI) concentration followed by decrease of absorption band intensity at 349 nm under irradiation in the presence of TiO_2/ZrO_2 films; simultaneously the absorption at 550 nm increases due to nontoxic Cr(III) formation.

Photocatalytic activity of mesoporous TiO_2 and TiO_2/ZrO_2 (5–30%) films, in comparison with films prepared without template, increases in accordance with increasing specific surface area of the samples (Table 1). The conversion of $Cr_2O_7^{2-}$, calculated for mesoporous TiO_2 films, was 4 times higher than that observed for nonporous samples, and 10 times higher than that reported in [24] for the equal amount of TiO_2, supported on hollow glass microbeads during the same time of irradiation.

Enhanced activity was observed for TiO_2/ZrO_2 films with low concentration of zirconium that possesses high surface area and composes of nanoparticles with mean size 3–4 nm. Zr doping retards not only anatase to rutile transformation, but also inhibits the crystalline growth [9, 10]. It can be seen that in general there is increase of E_g with the anodic shift of the upper edge of the valence band ΔE_v positions as the Zr concentration increases. Processes of EDTA oxidation accelerate, improving charge separation, and Cr(IV) reduction proceeds faster due to synergism between the oxidation and

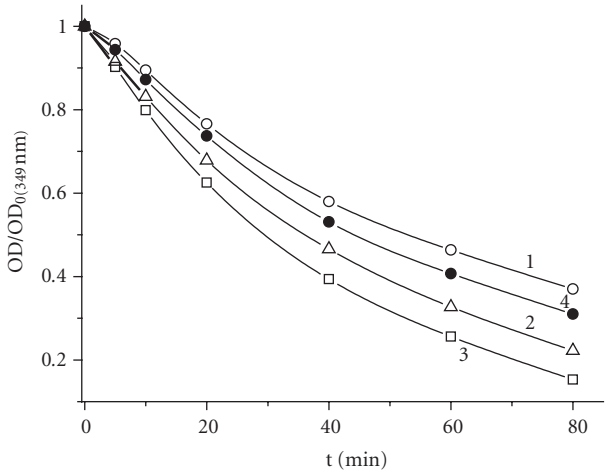

Figure 3: Normalized concentration versus time for Cr(VI) reduction over TiO_2 films: nonporous - 1, mesoporous - 2, and TiO_2/ZrO_2 films with 5% - 3 and 30% Zr content - 4 for 20 ml of $2 \cdot 10^{-4}$ M water solution of $K_2Cr_2O_7$ in the presence of EDTA ($2 \cdot 10^{-4}$ M) pH = 2 over 1 film (m = 0.001 g), $\lambda_{irrad.}$ = 254 nm, $P_0 = 3 \cdot 10^{-7}$ einstein $\cdot$ dm$^{-3} \cdot$ s^{-1}.

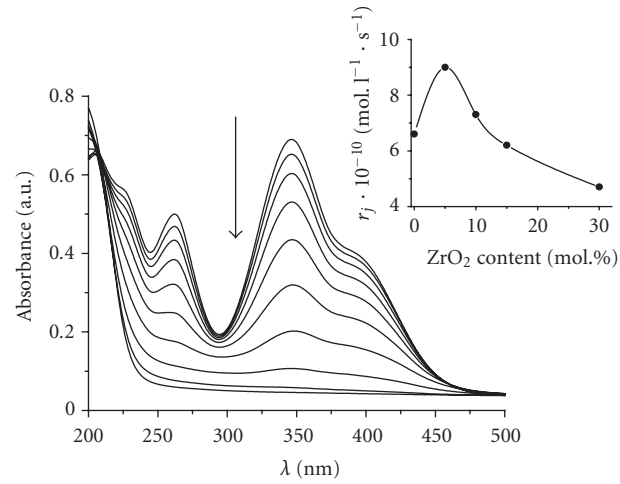

Figure 4: UV-Vis absorption spectra changes in 2,4-dinitroaniline ($5 \cdot 10^{-5}$ M) degradation under irradiation (λ = 254 nm, $P_0 = 3 \cdot 10^{-7}$ einstein $\cdot$ dm$^{-3} \cdot$ s^{-1}) in the presence of TiO_2/ZrO_2 (5%) film (m = 0.001 g). Spectra were registered every 30 min. Inset: initial reaction rates of photooxidation versus Zr concentration in TiO_2/ZrO_2 films.

reduction reactions. Further increasing of Zr content leads to low crystallinity of TiO_2/ZrO_2 (30%) and amorphous structure of TiO_2/ZrO_2 (50%) samples. This effect explains the drop of activity of TiO_2/ZrO_2 (30%) samples in comparison with pure TiO_2.

3.4. *Photocatalytic activity of* TiO_2/ZrO_2 *coatings in 2,4-dinitroaniline photooxidation*

The activity of the prepared samples in photooxidation processes was estimated in 2,4-dinitroaniline decomposition. The concentration of 2,4-dinitroaniline was calculated from the intensity of the adsorption band at 346 nm (Figure 4). During 2,4-dinitroaniline irradiation, overall decrease of absorption was observed. 2,4-dinitroaniline concentration decreased exponentially with time of irradiation. Process was followed by significant pH changes from 7 at the beginning to 4.8–4.3 (depending on the sample activity) after 3 hours of irradiation that can be assumed as completely mineralization of organic substrate accompanied with nitric acid, CO_2 and H_2O formation. NO_3^- formation was detected by increase of corresponding absorption band (203 nm). Qualitative reaction with diphenylamine gives characteristic for NO_3^- ions blue coloration [25].

On the base of literature [1, 2, 26], the heterogeneous photocatalytic process of degradation of 2,4-dinitroaniline can be expressed as follows:

$$TiO_2 \xrightarrow{h\nu} TiO_2(h^+ + e^-). \tag{2}$$

Photogenerated holes of valence band migrate to the surface. The oxidative pathway can be performed by direct hole attack or mediated by OH radicals, that formed when holes react with OH^- groups on the TiO_2 surface:

$$(TiO_2) \cdots OH^- + h^+ \longrightarrow \cdot OH. \tag{3}$$

Photoinduced electrons of conductive band interact with electron acceptors, generally dissolved O_2, which is transformed in superoxide radical anion $O_2 \cdot^-$. This radicals ($\cdot$OH, $O_2 \cdot^-$) possess high oxidative potential for complete mineralization of 2,4-dinitroaniline through organic intermediates to inorganic, $NO_3^- + CO_2 + H_2O$ [26]:

$$\begin{aligned} &\cdot OH/O_2 \cdot^- + 2,4\text{-dinitroaniline} \\ &\longrightarrow (\text{organic intermediates}) \\ &\longrightarrow NO_3^- + CO_2 + H_2O. \end{aligned} \tag{4}$$

For comparison of photoactivity of the samples, the rates of photooxidation were calculated in pseudo-first-order reaction approach [2] under equal conditions (Figure 4, inset). Mesoporous samples show enhanced activity (2–3 times) toward the coatings prepared without template. Highest activity in 2,4-dinitroaniline decomposition corresponds to TiO_2/ZrO_2 films with optimum 5–10% Zr concentration having nanocrystalline structure (crystal size 3–4 nm) with high step of crystallinity and high surface area.

4. CONCLUSIONS

Optically transparent, mesoporous TiO_2 and TiO_2/ZrO_2 thin film photocatalysts with stable porous structure were fabricated by sol-gel technique, using nonionic amphiphilic block copolymer Pluronic P123 as template.

Zr doping on the stage of sol-gel process improves thermal stability, retards sintering of the films, and stabilizes the nanocrystalline structure with developed porosity.

The E_g values obtained for mesoporous TiO_2/ZrO_2 films coincide with reported ones for nanostructured TiO_2 (anatase); mean particles size decreases with increasing of Zr content.

Whereas the flatband potentials of -0.52 V and bottom of conducting band edge position, measured for TiO_2 and for TiO_2/ZrO_2 versus NHE, differ insignificantly, enhancing of catalytic activity of zirconia-doped films originates from an anodic shift of the valence band edge.

Highest activity in photoreduction of Cr(VI) in the presence of EDTA as well as in the photooxidation process of 2,4-dinitroaniline decomposition corresponds to TiO_2/ZrO_2 films with optimum 5–10% Zr concentration, nanocrystalline structure (crystal sizes 3–4 nm), high degree of crystallinity (80%), and high surface area.

ACKNOWLEDGMENTS

The authors thank Dr. E. I. Oranskaja for XRD and W. Huang for SEM measurements.

REFERENCES

[1] M. R. Hoffmann, S. T. Martin, W. Choi, and D. W. Bahnemann, "Environmental applications of semiconductor photocatalysis," *Chemical Reviews*, vol. 95, no. 1, pp. 69–96, 1995.

[2] U. Siemon, D. W. Bahnemann, J. J. Testa, D. Rodrígues, M. I. Litter, and N. Bruno, "Heterogeneous photocatalytic reactions comparing TiO_2 and Pt/TiO_2," *Journal of Photochemistry and Photobiology A: Chemistry*, vol. 148, no. 1–3, pp. 247–255, 2002.

[3] T. López, R. Gómez, E. Sanchez, F. Tzompantzi, and L. Vera, "Photocatalytic activity in the 2,4-dinitroaniline decomposition over TiO2 sol-gel derived catalysts," *Journal of Sol-Gel Science and Technology*, vol. 22, no. 1-2, pp. 99–107, 2001.

[4] P. C. A. Alberius, K. L. Frindell, R. C. Hayward, E. J. Kramer, G. D. Stucky, and B. F. Chmelka, "General predictive syntheses of cubic, hexagonal, and lamellar silica and titania mesostructured thin films," *Chemistry of Materials*, vol. 14, no. 8, pp. 3284–3294, 2002.

[5] E. L. Crepaldi, G. J. Soler-Illia, D. Grosso, F. Cagnol, F. Ribot, and C. Sanchez, "Controlled formation of highly organized mesoporous titania thin films: from mesostructured hybrids to mesoporous nanoanatase TiO_2," *Journal of the American Chemical Society*, vol. 125, no. 32, pp. 9770–9786, 2003.

[6] R. Vogel, P. Meredith, I. Kartini, et al., "Mesostructured dye-doped titanium dioxide for micro-optoelectronic applications," *ChemPhysChem*, vol. 4, no. 6, pp. 595–603, 2003.

[7] J. C. Yu, J. Yu, and J. Zhao, "Enhanced photocatalytic activity of mesoporous and ordinary TiO_2 thin films by sulfuric acid treatment," *Applied Catalysis B: Environmental*, vol. 36, no. 1, pp. 31–43, 2002.

[8] M. E. Zorn, D. T. Tompkins, W. A. Zeltner, and M. A. Anderson, "Catalytic and photocatalytic oxidation of ethylene on titania-based thin-films," *Environmental Science & Technology*, vol. 34, no. 24, pp. 5206–5210, 2000.

[9] J. Kim, K. C. Song, S. Foncillas, and S. E. Pratsinis, "Dopants for synthesis of stable bimodally porous titania," *Journal of the European Ceramic Society*, vol. 21, no. 16, pp. 2863–2872, 2001.

[10] M. E. Manríquez, T. López, R. Gómez, and J. Navarrete, "Preparation of TiO_2-ZrO_2 mixed oxides with controlled acid-basic properties," *Journal of Molecular Catalysis A: Chemical*, vol. 220, no. 2, pp. 229–237, 2004.

[11] Yu. Gnatyuk, N. Smirnova, A. Eremenko, and V. Ilyin, "Design and photocatalytic activity of mesoporous TiO_2/ZrO_2 thin films," *Adsorption Science & Technology*, vol. 23, no. 6, pp. 497–508, 2005.

[12] X. Fu, L. A. Clark, Q. Yang, and M. A. Anderson, "Enhanced photocatalytic performance of titania-based binary metal oxides: TiO_2/SiO_2 and TiO_2/ZrO_2," *Environmental Science & Technology*, vol. 30, no. 2, pp. 647–653, 1996.

[13] A. Sclafani, L. Palmisano, and M. Schiavello, "Influence of the preparation methods of titanium dioxide on the photocatalytic degradation of phenol in aqueous dispersion," *The Journal of Physical Chemistry*, vol. 94, no. 2, pp. 829–832, 1990.

[14] N. Vityuk, Ya. Divinsky, N. Smirnova, and A. Eremenko, *Chemistry, Physics and Technology of Surfaces*, vol. 9, p. 71, 2003.

[15] S. J. Gregg and K. S. W. Sing, *Adsorption, Surface Area and Porosity*, Academic Press, London, UK, 1982.

[16] Ya. Gurevich and Yu. V. Pleskov, *Photoelectrochemistry of Semiconductors*, Nauka, Moscow, Russia, 1983.

[17] A. L. Linsebigler, G. Lu, and J. T. Yates Jr., "Photocatalysis on TiO2 surfaces: principles, mechanisms, and selected results," *Chemical Reviews*, vol. 95, no. 3, pp. 735–758, 1995.

[18] A. Hagfeldt and M. Grätzel, "Light-induced Redox reactions in nanocrystalline systems," *Chemical Reviews*, vol. 95, no. 1, pp. 49–68, 1995.

[19] S. Sakthivel and H. Kisch, "Photocatalytic and photoelectrochemical properties of nitrogen-doped titanium dioxide," *ChemPhysChem*, vol. 4, no. 5, pp. 487–490, 2003.

[20] L. Kavan, M. Grätzel, S. E. Gilbert, C. Klemenz, and H. J. Scheel, "Electrochemical and photoelectrochemical investigation of single-crystal anatase," *Journal of the American Chemical Society*, vol. 118, no. 28, pp. 6716–6723, 1996.

[21] Ye. V. Kuzminskii and G. Ya. Kolbasov, "Electrochemical systems for converting solar energy," *Solar Energy Materials & Solar Cells*, vol. 56, no. 2, pp. 93–115, 1999.

[22] G. Ya. Kolbasov, A. V. Sachenko, and I. I. Karpov, *Elektrokhimiya*, vol. 19, p. 1633, 1983.

[23] G. Colón, M. C. Hidalgo, and J. A. Navío, "Photocatalytic deactivation of commercial TiO_2 samples during simultaneous photoreduction of Cr(VI) and photooxidation of salicylic acid," *Journal of Photochemistry and Photobiology A: Chemistry*, vol. 138, no. 1, pp. 79–85, 2001.

[24] S.-F. Chen and X.-L. Chen, *Chinese Journal of Chemistry*, vol. 17, no. 4, p. 399, 1999.

[25] Yu. A. Kljachko and S. A. Shapiro, *Qualitative Chemical Analysis*, Goskhimizdat, Moscow, Russia, 1960.

[26] I. M. Arabatzis, T. Stergiopoulos, D. Andreeva, S. Kitova, S. G. Neophytides, and P. Falaras, "Characterization and photocatalytic activity of Au/TiO_2 thin films for azo-dye degradation," *Journal of Catalysis*, vol. 220, no. 1, pp. 127–135, 2003.